Oxygen stable isotopes during the Last Glacial Maximum climate: perspectives from data–model (iLOVECLIM) comparison

Thibaut Caley, Didier M. Roche, C. Waelbroeck, Elisabeth Michel

Clim. Past, 10, 1939–1955, 2014
www.clim-past.net/10/1939/2014/
doi:10.5194/cp-10-1939-2014

Climate of the Past
Open Access

Oxygen stable isotopes during the Last Glacial Maximum climate: perspectives from data–model (*i*LOVECLIM) comparison

T. Caley[1], **D. M. Roche**[1,2], **C. Waelbroeck**[2], **and E. Michel**[2]

[1]Earth and Climate Cluster, Faculty of Earth and Life Sciences, Vrije Universiteit Amsterdam, Amsterdam, The Netherlands
[2]Laboratoire des Sciences du Climat et de l'Environnement (LSCE), CEA/CNRS-INSU/UVSQ, Gif-sur-Yvette Cedex, France

Correspondence to: T. Caley (t.caley@vu.nl)

Received: 29 October 2013 – Published in Clim. Past Discuss.: 10 January 2014
Revised: 8 August 2014 – Accepted: 6 October 2014 – Published: 10 November 2014

Abstract. We use the fully coupled atmosphere–ocean three-dimensional model of intermediate complexity *i*LOVECLIM to simulate the climate and oxygen stable isotopic signal during the Last Glacial Maximum (LGM, 21 000 years). By using a model that is able to explicitly simulate the sensor (δ^{18}O), results can be directly compared with data from climatic archives in the different realms.

Our results indicate that *i*LOVECLIM reproduces well the main feature of the LGM climate in the atmospheric and oceanic components. The annual mean δ^{18}O in precipitation shows more depleted values in the northern and southern high latitudes during the LGM. The model reproduces very well the spatial gradient observed in ice core records over the Greenland ice sheet. We observe a general pattern toward more enriched values for continental calcite δ^{18}O in the model at the LGM, in agreement with speleothem data. This can be explained by both a general atmospheric cooling in the tropical and subtropical regions and a reduction in precipitation as confirmed by reconstruction derived from pollens and plant macrofossils.

Data–model comparison for sea surface temperature indicates that *i*LOVECLIM is capable to satisfyingly simulate the change in oceanic surface conditions between the LGM and present. Our data–model comparison for calcite δ^{18}O allows investigating the large discrepancies with respect to glacial temperatures recorded by different microfossil proxies in the North Atlantic region. The results argue for a strong mean annual cooling in the area south of Iceland and Greenland between the LGM and present (> 6 °C), supporting the foraminifera transfer function reconstruction but in disagreement with alkenones and dinocyst reconstructions. The data–model comparison also reveals that large positive calcite δ^{18}O anomaly in the Southern Ocean may be explained by an important cooling, although the driver of this pattern is unclear. We deduce a large positive δ^{18}Osw anomaly for the north Indian Ocean that contrasts with a large negative δ^{18}Osw anomaly in the China Sea between the LGM and the present. This pattern may be linked to changes in the hydrological cycle over these regions.

Our simulation of the deep ocean suggests that changes in δ^{18}Osw between the LGM and the present are not spatially homogeneous. This is supported by reconstructions derived from pore fluids in deep-sea sediments. The model underestimates the deep ocean cooling thus biasing the comparison with benthic calcite δ^{18}O data. Nonetheless, our data–model comparison supports a heterogeneous cooling of a few degrees (2–4 °C) in the LGM Ocean.

1 Introduction

Oxygen stable isotopes (δ^{18}O) are among the most widely used/common tools in palaeoclimatology–palaeoceanography. δ^{18}O constitutes an important tracer of the hydrological cycle for the different components of the climatic system (ocean, atmosphere, ice sheets) but processes that control the recorded δ^{18}O signal are various and complex. Simulation of climate and its associated isotopic signal allow an investigation of these various and complex processes (e.g. Roche et al., 2004a; Lewis et al., 2010).

Water isotopes have been implemented in numerous atmospheric and oceanic general circulation models (Jouzel et al., 1987; Joussame and Jouzel, 1993; Hoffmann et al.,

Table 1. δ^{18}O anomaly between the LGM and LH compiled for Greenland ice cores and speleothem records and compared to model (*i*LOVECLIM) results.

Site name	Latitude	Longitude	Elevation (m)	References	δ^{18}Op data LGM-LH (‰)	Error anomaly (2σ)	δ^{18}Op *i*LOVECLIM LGM-LH (‰)			
Camp century	77.18	−61.13	1887	Johnsen et al., 1972	−12.87		−13.38			
GISP	72.58	−38.48	3208	Grootes et al., 1997	−5.4	1.74	−2.32			
GRIP	72.57	−37.62	3232	Johnsen et al., 1997	−5.73	2.90	−2.32			
NGRIP	75.1	−42.32	2917	NGRIP Members, 2004	−7.18	2.06	−8.36			
Renland	72	−25	2340	Johnsen et al., 1992	−5		−2.75			
Dye 3	65.18	−43.81	2480	Langway et al., 1985	−4.5		−1.96			
					δ^{18}Oc Data LGM-LH (‰)		δ^{18}Oc *i*LOVECLIM LGM-LH (‰)	δ^{18}Oc Data LH (‰)	Error LH (2σ)	δ^{18}Oc *i*LOVECLIM LH (‰)
Botuverá Cave	−27.22	−49.16	230	Cruz et al., 2005	−0.34	0.52	0.55	−3.17	0.96	−4.84
Cold Air Cave	−24.02	29.11	1375	Holmgren et al., 1999	1.2	1.61	0.80	−4.08	1.34	−7.40
Gunung Buda National Park	4.03	114.8	150	Partin et al., 2007	1.73	0.42	1.66	−9.34	0.28	−6.43
Jerusalem West Cave	31.78	35.15	700	Frumkin et al., 1999	1.3	0.48	1.09	−4.84	0.30	−3.99
NWSI northwest of the South Island	−42	172	700	Williams et al., 2010	0.29	0.46	1.02	−3.20	0.30	−3.17
Sofular Cave	41.42	31.93	700	Fleitmann et al., 2009	−4.57	0.56	0.90	−8.08	0.46	−2.82
Soreq Cave	31.45	35.03	400	Bar-Matthews et al., 2003	2.11	0.47	1.09	−5.36	0.38	−3.99
Kesang Cave	42.87	81.75	2000	Cheng et al., 2012	1.72	1.81	5.19	−7.50	1.78	−10.10
Mt. Arthur	−41.28	172.63	390	Hellstrom et al., 1998	0.93	0.50	1.31	−6.14	0.28	−3.29
Namibia	−25	18		Stute and Talma, 1998	1.5		1.50	−7.20	0.40	−4.63
Rio Grande do Norte	−5.6	−37.73	100	Cruz et al., 2009	0		2.38	−2.00		−8.40
Santana Cave	−24.52	−48.72	700	Cruz et al., 2006	−1.7		0.9	−5.00		−8.40

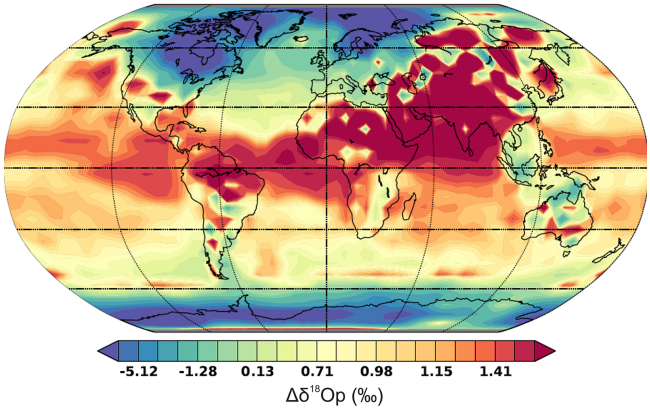

Figure 1. Simulated precipitation δ^{18}O anomaly (LGM-CT) in *i*LOVECLIM. The colour scale is based on the distribution of the values in the data set used: 95 % of the proxy data are meant to be appropriately represented in that colour scale. It is centred around the mean of the data set, hence red represents heavier values than the mean and blue represents lighter values than the mean of the data set.

1998; Schmidt, 1998; Paul et al., 1999; Delaygue et al., 2000; Werner et al., 2000; Noone and Simmonds, 2002; Mathieu et al., 2002; Lee et al., 2007; Yoshimura et al., 2008; Zhou et al., 2008; Tindall et al., 2009; Risi et al., 2010; Werner et al., 2011; Xu et al., 2012). However, they have very seldom been used in coupled climate simulations with water isotopes in both the atmospheric and oceanic components, due to computational costs (Schmidt et al., 2007; LeGrande and Schmidt, 2011). We chose here to use an intermediate complexity model to circumvent that limitation, while retaining a full oceanic general circulation model to allow investigating the details of the oceanic response where numerous palaeodata are available.

Water isotopes have been implemented and validated against data for the present day climate in the global three-dimensional model of intermediate complexity *i*LOVECLIM (Roche, 2013; Roche and Caley, 2013; Caley and Roche, 2013). In the present study, we focus on the Last Glacial Maximum (LGM) climate, a cold climatic extreme. We will refer to the LGM as the period around 21 thousand years before present because (1) it is coherent with the commonly used time period in previous climate simulations and (2) it has been defined as the period between 23 and 19 thousand years before present based on a thorough examination of palaeoclimatic data (Mix et al., 2001). To our knowledge, the present study is the first attempt at a global atmosphere–ocean coupled simulation of the Last Glacial Maximum with isotopes in both components and with an oceanic general circulation model. One earlier coupled model study including oxygen isotopes used a spatially greatly simplified model (Roche et al., 2004b).

The LGM has become a standard target period to constrain climate sensitivity and evaluate a model's capability to simulate a climate that is drastically different from that of the present day. Efforts have been made to improve multi-model intercomparisons under glacial boundary conditions to diagnose the range of possible responses, to a given change in forcing. These efforts have been realized by the pioneering work of the Palaeoclimate Modeling Intercomparison Project (PMIP). PMIP used Atmospheric General Circulation models (Joussaume and Taylor, 2000) in its first phase, and Coupled Atmospheric–Ocean models in its second phase (PMIP2) (Crucifix et al., 2005; Braconnot et al., 2007a, b). PMIP is now in its third phase (CMIP5/PMIP3 palaeo-simulations) and uses a coherent framework between past, present and future simulations to provide a systematic and quantitative assessment of the realism of the models used to predict the future (Braconnot et al., 2012; Schmidt et al., 2014).

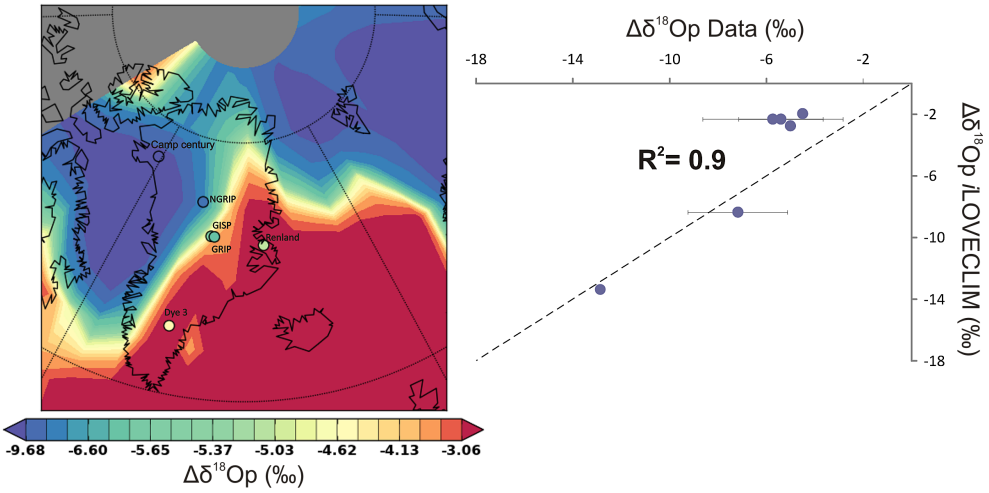

Figure 2. Comparison between simulated precipitation δ^{18}O anomaly (LGM-CT) in *i*LOVECLIM and ice core data from Greenland (Table 1). Reported uncertainties on data are 2σ. For colour scale generation explanations see Fig. 1 caption.

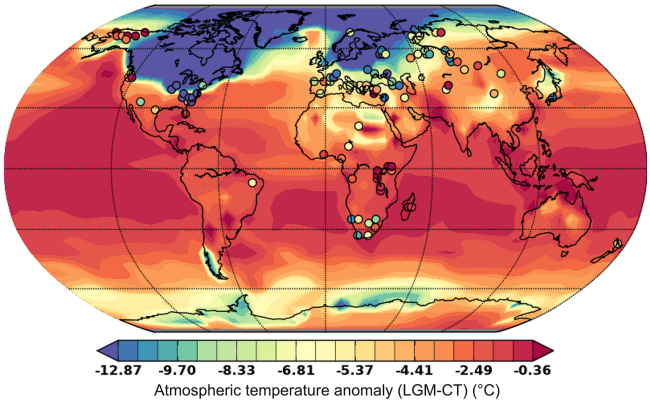

Figure 3. Comparison between simulated atmospheric temperature anomaly (LGM-CT) in *i*LOVECLIM and pollen-based continental climate reconstructions (Bartlein et al., 2011). For colour scale generation explanations see Fig. 1 caption.

The evaluations of model results are supported by environmental proxy data that have been compiled in several projects aimed at the reconstruction of the LGM surface conditions, like Climate Long-Range Investigation Mapping and Prediction (CLIMAP, 1981), Glacial Atlantic Mapping and Prediction (GLAMAP, 2000: Sarnthein et al., 2003) and more recently The Multiproxy Approach for the Reconstruction of the Glacial Ocean Surface (MARGO, Kucera et al., 2005; MARGO Project Members, 2009). However, all environmental proxies are influenced by non-climatic factors and/or further climatic factors. A promising way of exploiting palaeoenvironmental data for climate-model evaluation is to use models that explicitly simulate the sensor. A decisive advantage of isotope-enabled models is their ability to directly simulate measured quantities (in the present case, δ^{18}O), so that their results can be directly compared with data from the different climatic archives.

In this study, we present a comparison between LGM simulated and measured oxygen isotopes. The results are presented in terms of anomaly between the LGM and the present. The use of anomaly renders absolute values irrelevant; it concerns a purely relative change. We can therefore ignore complications such as species-specific climate variable relationships, vital effect offsets (Rohling and Cooke, 1999) and non-calibration problems between laboratories. We consider both the atmospheric and oceanic component and discuss the agreement between data and model results, as well as the processes driving the isotopic signal recorded.

2 Material and method

2.1 The *i*LOVECLIM model

The *i*LOVECLIM (version 1.0) model is a derivative of the LOVECLIM-1.2 climate model extensively described in Goosse et al. (2010). From the original model, we retain the atmospheric (ECBilt), oceanic (CLIO), vegetation (VECODE) and land surface (LBM) components and develop a complete, conservative, water isotope cycle through all cited components. A detailed description of the method used to compute the oxygen isotopes in *i*LOVECLIM can be found in Roche (2013) and the validation of model results can be found in Roche and Caley (2013) and Caley and Roche (2013). With regard to water isotopes, the main development lies in the atmospheric component (approximately 5.6° resolution in latitude and longitude) in which evaporation, condensation and existence of different phases (liquid and solid) all affect the isotopic conditions of the water isotopes. In the ocean (approximately 3° resolution in latitude and

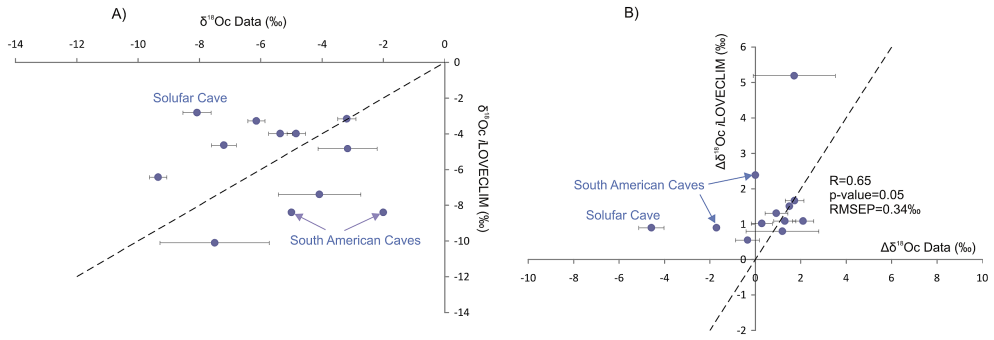

Figure 4. (a) Comparison between simulated continental calcite δ^{18}O for the present day (CT) in *i*LOVECLIM and global speleothem data (Table 1). **(b)** Comparison between simulated continental calcite δ^{18}O anomaly (LGM-CT) in *i*LOVECLIM and global speleothem data (Table 1). Reported uncertainties on data are 2σ. The quantification of model–data agreement ($R = 0.65$; p value $= 0.05$; RMSEP $= 0.34$ ‰) is based on nine records (Solufar, Rio Grande do Norte and Santana Cave records were excluded).

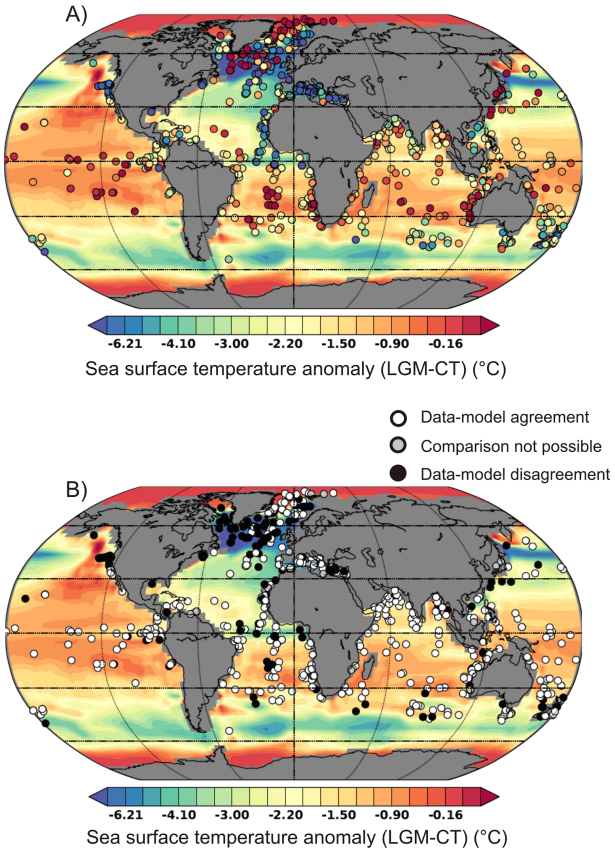

Figure 5. (a) Comparison between simulated SST anomaly (LGM-CT) in *i*LOVECLIM and MARGO data (MARGO Project Members, 2009). **(b)** Quantitative agreement or disagreement between simulated SST anomaly (LGM-CT) in *i*LOVECLIM and MARGO data (MARGO Project Members, 2009), taking into account the uncertainties on SST reconstructions. Grey points (comparison not possible) denote the absence of error bars on data or denote locations where model results are not comparable to data (coastal sites). For colour scale generation explanations see Fig. 1 caption.

longitude), the water isotopes are acting as passive tracers ignoring the small fractionation implied by the presence of sea-ice (Craig and Gordon, 1965). For the land surface model, the implementation in the bucket follows the same procedure as for the water except that equilibrium fractionation is assumed during phase changes. The isotopic fields simulated are shown to reproduce most expected δ^{18}O–climate relationships with the notable exception of the isotopic composition in Antarctica.

2.2 LGM boundary conditions

We use the boundary conditions defined in/by the PMIP2 protocol to simulate the LGM climate. Lowered levels of atmospheric greenhouse gas concentrations ($CO_2 = 185$ ppm, $CH_4 = 350$ ppb and $NO_2 = 200$ ppb) are used in agreement with ice-core measurements (Fluckiger et al., 1999; Dällenbach et al., 2000; Monnin et al., 2001). Ice-sheet topography changes are taken from Peltier (2004) and the surface albedo is set accordingly. Orbital parameters correspond to 21 000 years before present (Berger and Loutre, 1992). To account for the ~ 130 m decrease in sea level relative to the present day, the land–sea mask and the oceanic bathymetry are modified (Lambeck and Chappell, 2001). Some variations exist among the PMIP simulations, mainly for the Northern Hemisphere, in the handling of changes in the river basins (Weber et al., 2007), i.e. changes in river routing due to the presence of ice sheets. In our LGM simulation we included changes in the water routing from the Laurentide ice sheet over North America and from the Fennoscandian ice sheet over Eurasia. River routing is computed following the topography using the largest slope until the sea is reached. No lakes are allowed and a depression is forced to drain into the closest cell that itself drains into the sea. We applied the above forcings to the model's equilibrium state and integrated it until a new equilibrium was reached, after 5000 years of integration. We ran the model long enough so that deep Pacific waters (bottom layer of our ocean model) do not show any visible trend

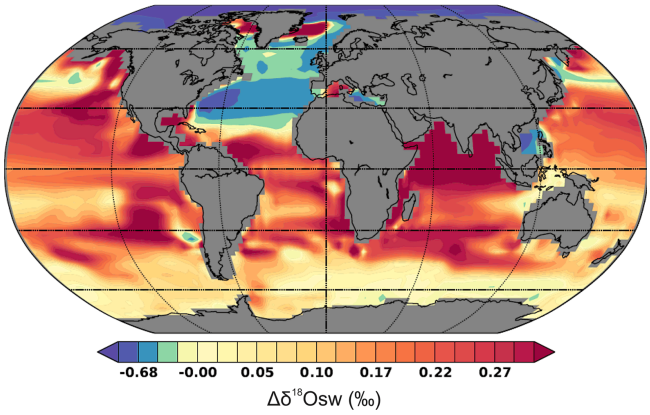

Figure 6. Simulated surface water δ^{18}O anomaly (LGM-CT) in *i*LOVECLIM. A correction of the LGM ice sheet contribution (1 ‰) has been applied. For colour scale generation explanations see Fig. 1 caption.

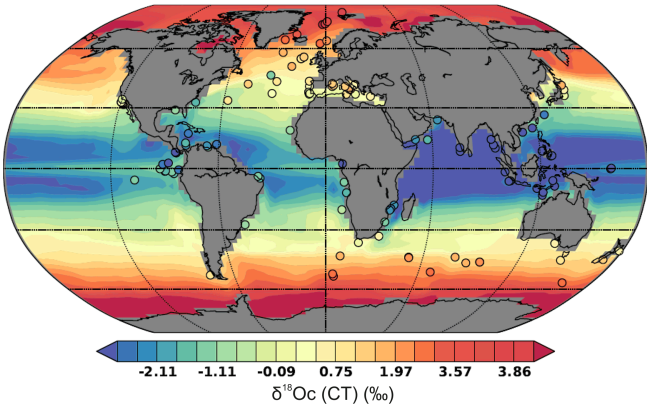

Figure 7. Comparison between simulated surface ocean calcite δ^{18}O for the present day (CT) in *i*LOVECLIM (0–50 m) (Caley and Roche, 2013) and global planktic foraminifera data (Table S1). For colour scale generation explanations see Fig. 1 caption.

on a millennial timescale basis. Deep temperatures in the Pacific are changing by less than 0.001 °C per millennium in the mean, while the decadal variability of the model in the same area and over the same part of the simulation is 0.01 °C (at 5000 m depth). Trends in δ^{18}O are of the same order of magnitude.

Our choice of using the PMIP2 boundary conditions instead of the more recent PMIP3 protocol arises from several considerations: (1) having a state readily comparable to the already published LGM state of an earlier version of the model (Roche et al., 2007), (2) the possibility in a future study to intercompare our atmospheric results to already published PMIP2 LGM atmospheric general circulation model (3) the fact that the main difference between the PMIP2 and PMIP3 protocols is in the ice sheet elevation (http://pmip3.lsce.ipsl.fr) which, interpolated on our atmospheric coarse resolution grid, is not very large.

2.3 Global data sets compilation

Global oxygen isotopic data sets for the atmospheric and oceanic components have been already compiled for the Late Holocene (LH) and have been compared and discussed with *i*LOVECLIM results (Caley and Roche, 2013). Here we compiled δ^{18}O data at sites for which the LGM interval is available in order to calculate signal anomalies. Table 1 is a compilation of δ^{18}O data from six published records from Greenland ice cores. The ice δ^{18}O anomalies are reported as the difference between averaged δ^{18}O values computed over the period 20 000–22 000 years BP and over the last 1000 years of each record, using published chronologies. Table 1 also includes calcite δ^{18}O data from 12 published speleothem records. We compiled only the speleothem records that cover both the LGM and LH time interval. Calcite δ^{18}O anomalies are reported as the difference between averaged δ^{18}O values computed over the period 20 000–22 000 years BP and over the last 1000 years of each record, using published U/Th chronologies.

We compiled calcite δ^{18}O measurements from 114 pairs of deep-sea cores for which both LGM and LH planktic foraminifera δ^{18}O exist and from 114 pairs of deep-sea cores for which benthic foraminifera δ^{18}O exist. Anomalies are reported as the difference between averaged δ^{18}O values computed over the period 19 000–23 000 years BP and over the last 3000 years of each record (Table S1 and S2 in the Supplement). Chronostratigraphic quality has been defined following the MARGO project definition (Kucera et al., 2005) (Table S1 and S2). The database composed of planktic and benthic foraminifera calcite δ^{18}O measurements of deep-sea cores is available at PANGAEA (Data set doi:10.1594/PANGAEA.836033).

Concerning planktic foraminifera, we worked with δ^{18}O data of the most commonly measured planktic foraminifer species: *Globigerinoides ruber white* and *pink*, *Globigerinoides sacculifer*, *Globigerina bulloides*, and *Neogloboquadrina pachyderma* sinistral for the majority of the sites (Waelbroeck et al., 2005). Two exceptions occur at sites MD96-2077 and OCE326-GGC5 for which *Globorotalia inflata* is used (Table S1). We extended our data set with 10 calcite δ^{18}O measurements of planktic foraminifera *Neogloboquadrina pachyderma* sinistral compiled by Meland et al. (2005). We only selected records for which the LGM level was determined by AMS ^{14}C and for which LH data (last 3000 years) was available. These authors used a definition for the LGM chronozone slightly different (18–21.5 ka) but the data allow comparison with model results in the Nordic seas, an area poorly documented in our compilation (Table S1).

Concerning benthic foraminifera δ^{18}O, we extended our data set with 22 calcite δ^{18}O measurements compiled by Zarriess and Mackensen (2011). These authors used

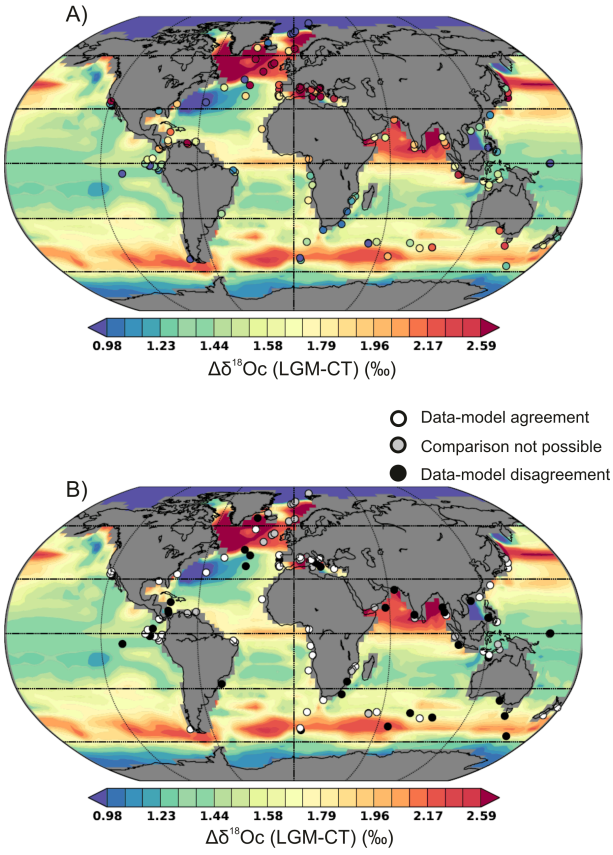

Figure 8. (a) Comparison between simulated surface ocean calcite δ^{18}O anomaly (LGM-CT) in *i*LOVECLIM (0–50 m) and global planktic foraminifera data (Table S1). **(b)** Quantitative agreement or disagreement between simulated surface ocean calcite δ^{18}O anomaly (LGM-CT) in *i*LOVECLIM (0–50 m) and global planktic foraminifera data (Table S1), taking into account the uncertainties on calcite δ^{18}O data (2σ). Grey points (comparison not possible) denote the absence of error bars on data or denote locations where model results are not comparable to data (coastal sites). For colour scale generation explanations see Fig. 1 caption.

a definition for the LGM chronozone (18.3–23.5 ka) that encompasses the one we used (19–23 ka). We also considered four calcite δ^{18}O measurements from Adkins et al. (2002) and two calcite δ^{18}O measurements from Malone et al. (2004) that have been combined in the same cores with pore fluids measurements in deep-sea sediments to reconstruct deep ocean temperature.

3 Results and discussion

3.1 Atmospheric component

3.1.1 Oxygen stable isotopes in precipitation

In the following we only briefly discuss the annual mean distribution of δ^{18}O in precipitation, since a complete description and intercomparison with previously published LGM δ^{18}O in precipitation simulations will be undertaken in another study/article in preparation.

Isotopic values are expressed relative to a standard (Sharp, 2007):

$$\delta^{18}\mathrm{O} = R(^{18}\mathrm{O})_\mathrm{p}/R(^{18}\mathrm{O})_\mathrm{std} - 1 \quad (1)$$

where R is the abundance ratio of the heavy and light isotopes – e.g. $\mathrm{N}(^{18}\mathrm{O})_\mathrm{p}\,/\,\mathrm{N}(^{16}\mathrm{O})_\mathrm{p}$ – for substance P and δ is commonly reported in units of parts per thousand (‰). The standard for carbonate is Pee Dee Belemnite (PDB) (Craig, 1957) and that for water is Standard Mean Ocean Water (SMOW) (Baertschi, 1976).

Model results for the annual mean precipitation δ^{18}O anomaly show large negative values in the northern and southern high latitudes at the LGM compared to the present (Fig. 1). Particularly visible are the area of very depleted δ^{18}O precipitation over the imposed LGM ice sheet in North America and northern Eurasia. In contrast, the mid-latitudes are only slightly depleted and the tropical regions slightly enriched. Over the oceans and with the notable exception of the North Atlantic, the anomaly is relatively symmetric with respect to the equator. Some areas over Siberia exhibit a surprisingly large positive anomaly, despite their increased continentality and the negative δ^{18}O anomaly in western Europe. We do not consider this result as valid but rather, as a result of a model deficiency at very low moisture content, a deficiency that has already been noted for the present day (Roche, 2013).

To compare our model results with isotopic data, we use the precipitation δ^{18}O signal from ice cores. We focus on Greenland ice cores (Table 1).

For the Greenland ice sheet, *i*LOVECLIM model result and data anomalies are in very good agreement ($R^2 = 0.9$) (Fig. 2). A gradient from weak negative δ^{18}O anomalies from the northwest (Camp Century) through the centre (GRIP, NGRIP) towards large negative δ^{18}O anomalies in the southeast (Dye-3) is visible in both data and model results. The maximum depletion occurs in our model over Baffin Bay, with a strong effect of glacial/interglacial sea-ice changes.

Concerning Antarctica, a numerical issue in the advection–diffusion scheme at very low humidity content (Roche, 2013) hampers a good data–model comparison.

Some tropical ice cores exist in the Himalayan (Dunde, Guliya) and Andes regions (Huascaran, Sajama and Illimani). The Tropics are marked by slightly positive δ^{18}O anomalies or no change in *i*LOVECLIM (Fig. 1). The model fails to simulate the depletions ranging from -2 to -5 ‰ inferred from tropical ice cores (Thompson et al., 1989, 1995, 1998, 2000; Ramirez et al., 2003; Risi et al., 2010). Part of the explanation could reside in the extreme altitude (around 5000–6000 m) of tropical ice cores, hampering a good data–model comparison. Indeed, the altitude in our coarse resolution model for these regions is lower (300 m for Andes and 4000 m for Himalaya). Another reason might be

the complex precipitation setting of the Andes, with a combination of moisture from the Pacific and recycled moisture from inland regions (Risi et al., 2010).

3.1.2 Oxygen stable isotopes in continental carbonates (speleothems)

Under equilibrium conditions, the δ^{18}O of continental carbonates (speleothems) depends on both the temperature through its control on equilibrium fractionation between water and calcite (Hendy, 1971; Kim and O'Neil, 1997) and the isotopic composition of drip water, from the cave site in which the speleothem grew, itself linked to the δ^{18}O in precipitation. This relationship between the δ^{18}O of carbonates, the δ^{18}O of the water, and temperature is expressed by the equation of Kim and O'Neil (1997) for synthetic calcite:

$$\delta^{18}\mathrm{O}_{\mathrm{calcite}}\,(\mathrm{speleothem}) = \delta^{18}\mathrm{O}_{\mathrm{water}} + (18.03 \cdot (1000/T) - 32.17) \quad (2)$$

where T is the temperature in Kelvin.

Although recent works suggest that calcite speleothems do not precipitate under equilibrium conditions (Mickler et al., 2006; Daeron et al., 2011), the use of anomaly calculations between the LGM and LH would limit such potential bias.

As the atmospheric temperature is an important control on the calcite δ^{18}O signal, we need to assess the modelled atmospheric temperature. To do so, we used the pollen-based continental climate reconstructions (Bartlein et al., 2011) (Fig. 3). A general cooling during the LGM is observed in both data and model results. Close to the Northern Hemisphere ice sheets the cooling is largest and well reproduced by the model. The LGM cooling indicated by pollen data is more pronounced in southern Europe in comparison to model results. This aspect was already noted (Vandenberghe et al., 2012) and was shown to reflect a too-little southward extension of winter sea-ice along the western European coast. It could be attributed to (1) the low resolution of the atmospheric component and (2) the absence of Gibraltar in the oceanic part of the model (Roche and Caley, 2013), promoting warm waters from the Mediterranean along the European coast (Roche et al., 2007; Vandenberghe et al., 2012). In the Tropics, the cooling is reduced compared to the high northern latitudes. With the exception of South Africa where a lot of scatter is observed in the data from a large cooling of -10 to a moderate -2 °C cooling, *i*LOVECLIM reproduces very well the main features of atmospheric temperature between the LGM and present.

Simulated atmospheric temperature and precipitation δ^{18}O are used to calculate calcite δ^{18}O. Data and model results for the present day, when error bars are considered, are relatively close to the 1 : 1 regression line, except for Solufar Cave and for South American speleothems (Fig. 4a). There is probably some bias due to limitation of the model together with the processes operating in the atmosphere, soil zone, epikarst and cave system that hamper a good quantitative data–model comparison for the calcite δ^{18}O signal as already observed with a larger database (Caley and Roche, 2013). To test whether these biases are climate-independent constant terms, the simulated annual mean anomaly between the LGM and the present is then compared to speleothem data (Fig. 4b). Considering the error bars on the data (Table 1), we observe overall positive calcite δ^{18}O anomalies except for Solufar Cave and South American caves (Fig. 5). For South America, there is a failure in *i*LOVECLIM to simulate lower δ^{18}Op (Fig. 1) as also observed in other GCMs (Jouzel et al., 2000; Werner et al., 2001; Risi et al., 2010). Whether the reason for that enrichment is the same in all models with such different complexities is not evident however. To understand fully the processes behind these δ^{18}Op changes would require an in-depth comparison of the models which has never been attempted so far.

As shown previously, mean annual atmospheric temperature is globally cooler during the LGM (Fig. 3). Precipitation reconstruction derived from subfossil pollens and plant macrofossils for the LGM suggests a significant decrease in precipitation compared to the present over Eurasia, Africa and North America (Bartlein et al., 2011). Both the significant cooling and drying of the LGM climate can explain the overall pattern toward positive calcite δ^{18}O anomalies. Overall, for 9 sites of the 12 compiled, there is a very good agreement between data and model results ($R = 0.65$; p value $= 0.05$; RMSEP $= 0.34$ ‰) (Fig. 4b). In a previous data–model comparison study for the late Holocene (Caley and Roche, 2013), we concluded that limitation of the model together with the processes operating in the atmosphere, soil zone, epikarst and cave system hampered a good quantitative data–model comparison for the continental calcite δ^{18}O signal. The better agreement between data and model results in terms of annual mean anomaly suggests that (1) this approach allows us to reduce complications with the atmospheric, soil and cave processes, (2) the bias in absolute calcite δ^{18}O values was probably a climate-independent constant term and (3) the model is capable of reproducing the right amplitude of changes. This offers new perspectives for the understanding of speleothem records covering the glacial–interglacial timescale. Indeed, long-term transient simulation of water isotopes with *i*LOVECLIM could be realized and the relationship between the δ^{18}O precipitation signal and climate variables such as temperature and precipitation rates could be investigated.

3.2 Surface and deep ocean

3.2.1 Oxygen stable isotopes in surface ocean carbonates (planktic foraminifera)

The carbonate isotopic concentration from various organisms such as foraminifera is mainly controlled by temperature and by the isotopic composition of seawater (δ^{18}Osw) during shell formation (Urey, 1947; Shackleton, 1974).

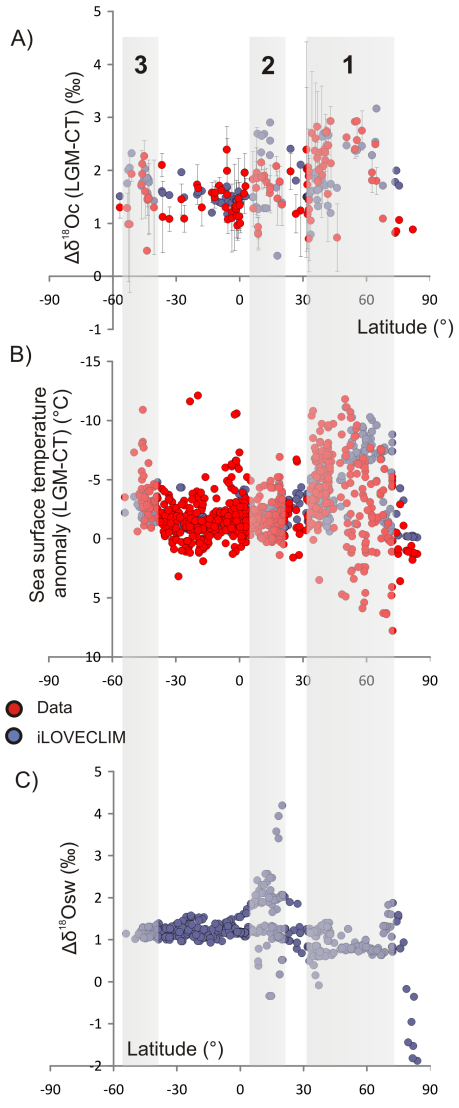

Figure 9. Data–model (*i*LOVECLIM) comparison as a function of latitude for **(a)** the surface ocean (0–50 m) calcite δ^{18}O anomaly (LGM-CT) and **(b)** sea surface temperature anomaly (LGM-CT). **(c)** Simulated surface water δ^{18}O anomaly (LGM-CT) in *i*LOVECLIM as a function of latitude (model results are taken at the same location as sea surface temperature data). Grey bands denote large positive calcite δ^{18}O anomaly in (1) the North Atlantic, (2) the North Indian Ocean and (3) the Southern Ocean as discussed in the text.

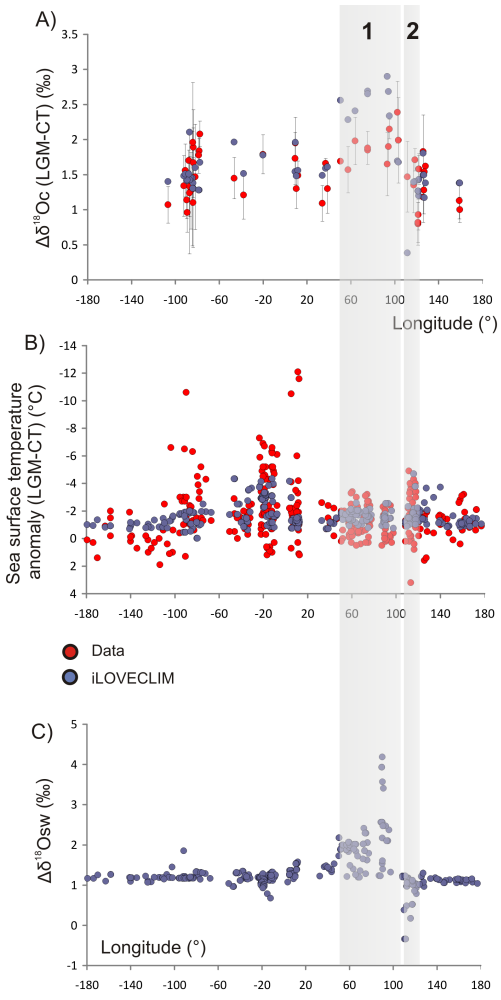

Figure 10. Data–model (*i*LOVECLIM) comparison as a function of longitude in the tropical band (30° N–30° S) for **(a)** the surface ocean (0–50 m) calcite δ^{18}O anomaly (LGM-CT) and **(b)** sea surface temperature anomaly (LGM-CT). **(c)** Simulated surface water δ^{18}O anomaly (LGM-CT) in *i*LOVECLIM as a function of longitude in the tropical area (30° N–30° S) (model results are taken at the same location as sea surface temperature data). Grey bands denote large positive/negative calcite δ^{18}O anomaly in (1) the North Indian Ocean and (2) the China Sea as discussed in the text.

The temperature dependence of the equilibrium fractionation of inorganic calcite precipitation around 16.9 °C is given in Shackleton (1974) as

$$T = 16.9 - 4.38\left(\delta^{18}\mathrm{O}_{\mathrm{carbonate(PDB)}} - \delta^{18}\mathrm{O}_{\mathrm{sw(SMOW)}}\right) + 0.1\left(\delta^{18}\mathrm{O}_{\mathrm{carbonate(PDB)}} - \delta^{18}\mathrm{O}_{\mathrm{sw(SMOW)}}\right)^2. \quad (3)$$

As the calcite δ^{18}O signal is controlled by temperature and δ^{18}Osw, it is important to discuss and assess these variables in our model. The assessment can be carried out for sea surface temperature (SST) using reconstruction of LGM SST derived from different microfossil proxies (MARGO Project Members, 2009). In contrast, there is currently no method to directly reconstruct surface water δ^{18}O in the past.

We observe a very good agreement between simulated and measured SST anomalies between the LGM and the present (Fig. 5). Figure 5b illustrates the data–model agreement or disagreement taking into account the uncertainties on LGM SST reconstructions (MARGO Project Members, 2009). Model results confirm that the strongest annual mean cooling occurred in the mid-latitude North Atlantic (MARGO Project

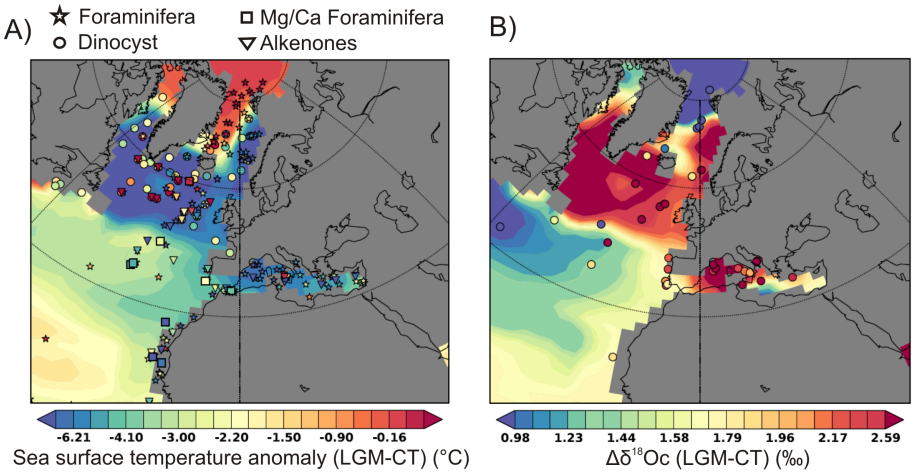

Figure 11. A focus on the North Atlantic region with **(a)** the comparison between simulated SST anomaly (LGM-CT) in *i*LOVECLIM and MARGO reconstructions for each temperature proxy (MARGO Project Members, 2009). **(b)** The comparison between simulated surface ocean calcite δ^{18}O anomaly (LGM-CT) in *i*LOVECLIM (0–50 m) and planktic foraminifera δ^{18}O data (Table S1). For colour scale generation explanations see Fig. 1 caption.

Members, 2009). However, some discrepancies between SST reconstructions and model results occur south of Iceland and Greenland. We discuss this point in detail later. In the tropical band (30° S–30° N) our model results are in excellent agreement with data and therefore confirm that the tropical cooling is more extensive than that proposed by CLIMAP (MARGO Project Members, 2009). Interbasin differences as well as west–east gradients within each basin, although much weaker in the model, mark the equatorial oceans in agreement with MARGO reconstructions.

After subtraction of the LGM ice sheet contribution ($\sim$ 1 ‰) (Schrag et al., 1996; Duplessy et al., 2002), modelled surface water δ^{18}O anomalies exhibit negative values in the North Atlantic region (between 30–60° N) (Fig. 6). This probably reflects the changes in ice sheets' distribution and their impact on surface water δ^{18}O through depleted water discharges from rivers. Both sides of the Greenland ice sheet are marked by positive anomalies (Fig. 6) that reflect the change from present day seasonal sea-ice to LGM permanent sea ice condition in agreement with proxy reconstruction (De Vernal et al., 2006). Changes in $\Delta\delta^{18}$Osw are null in the Southern Ocean and the rest of the oceans (tropical area) are mainly marked by slight positive anomalies, probably reflecting the more enriched δ^{18}O precipitation signal during the LGM (Fig. 1).

We computed annual mean calcite δ^{18}O from simulated δ^{18}Osw and SST and compared the results with deep-sea core data. Data and model results for the present day show an excellent agreement (Fig. 7) as already observed with a larger database (Caley and Roche, 2013). We chose a depth habitat of 0–50 m to calculate calcite δ^{18}O anomalies as we previously demonstrated that it was suitable for a comparison with a global and varied data set composed of different species of foraminifera (Caley and Roche, 2013) (Figs. 7 and 8). Although ecological effects can also play a role and are more expressed when individual species are considered (Caley and Roche, 2013) our strategy based on anomaly calculation limits such potential biases.

We observe a good qualitative agreement between data and model results (Fig. 8b). Figure 8b illustrates the data–model agreement or disagreement taking into account the uncertainties (2σ) on LGM and LH calcite δ^{18}O reconstructions (Table S1). Overall, we observe quantitative good agreement between data and model except in the North Indian region. Although calcite δ^{18}O anomalies are larger in the model than in the data, the sign of the latitudinal gradient observed in the Indian Ocean is correct (Fig. 8a).

Steep calcite δ^{18}O gradients between 30 and 90° N in the Atlantic Ocean are visible (Fig. 8). This is also expressed on a global latitudinal transect as the majority of data northward of 30° N are located in the Atlantic. The calcite δ^{18}O anomaly at 30° N is 1 ‰, then changes to 2.5–3 ‰ between 40 and 60° N and finally decreases to between 65 and 90° N (lower than 1 ‰) (Fig. 9a).

We compare these trends with a global latitudinal transect of ΔSST and the same latitudinal transect for the simulated $\Delta\delta^{18}$Osw (Fig. 9b and c). We conclude that observed calcite δ^{18}O gradients in the North Atlantic are mainly an effect of SST changes with latitude. Indeed, large positive calcite δ^{18}O anomalies are associated with negative δ^{18}Osw anomalies and colder temperatures indicating the dominant role of SST in driving the calcite δ^{18}O signal (Fig. 9).

The data–model comparison also reveals large positive calcite δ^{18}O anomalies in the Southern Ocean, between 45–50° S (1.5–2 ‰). In a previous study, we argue that a data–model comparison for calcite δ^{18}O in past climate could

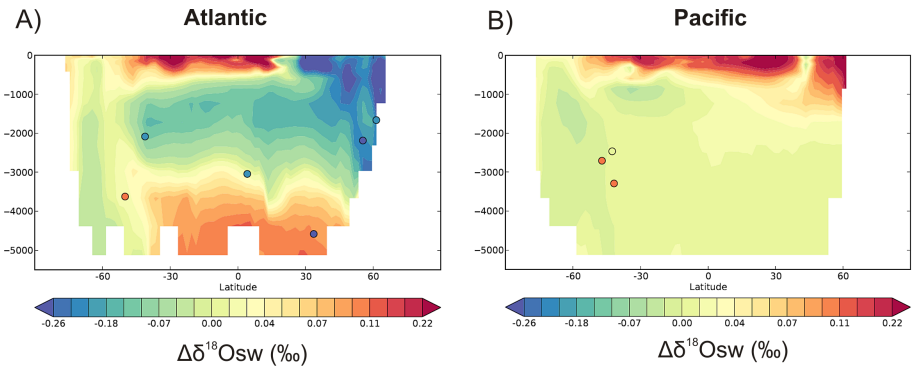

Figure 12. (a) Atlantic and **(b)** Pacific zonal mean anomaly (LGM-CT) for simulated deep water δ^{18}O in *i*LOVECLIM and water δ^{18}O in pore fluids of deep-sea sediments (Adkins et al., 2002; Schrag et al., 2002; Malone et al., 2004). A correction of the LGM ice sheet contribution (1 ‰) has been applied. For colour scale generation explanations see Fig. 1 caption.

constitute an interesting way for mapping the potential shifts of the frontal systems and circulation changes through time, in particular in the Southern region (Caley and Roche, 2013). The large values observed are linked to a large negative SST anomaly in the region with weak changes in $\Delta\delta^{18}$Osw observed in our model (Fig. 9). The cooling could be directly linked to the reorganization of frontal systems during glacial periods as documented in many studies (Peeters et al., 2004; Bard and Rickaby, 2009; Caley et al., 2012). However, the driver of this potential fronts reorganization is far from being understood. It could be related to SH westerlies changes, although recent data–model comparison works reached no clear conclusion on the behaviour of westerlies during the LGM (Kohfeld et al., 2013; Sime et al., 2013). It is interesting to note that the Southern Ocean, subtropical South Atlantic and Pacific are regions where large disagreements occur among the latest coupled-GCM LGM simulations (Braconnot et al., 2007a). The fact that *i*LOVECLIM reproduces well the observed cooling and the main pattern of the calcite δ^{18}O signal in the Southern region illustrates how data–model comparison for oxygen isotopes can serve to evaluate a model's capability to simulate a climate that is drastically different from that of the present day.

The tropical regions (30° N–30° S) exhibit overall a large positive calcite δ^{18}O anomaly of 1–2 ‰ that mainly reflects a negative SST anomaly (Figs. 9 and 10). An exception occurs in the North Indian Ocean for which we observed a higher calcite δ^{18}O anomaly (2–3 ‰). This anomaly cannot be explained by the cooling observed in the region – but rather by a higher $\Delta\delta^{18}$Osw (Figs. 9 and 10). Indeed, the cooling in the tropical Atlantic is more pronounced than in the North Indian Ocean but the calcite δ^{18}O anomaly is not larger (Fig. 10). This large positive anomaly observed in data for the North Indian Ocean is overestimated in the model (Figs. 8–10). This is probably due to the anomalously low δ^{18}Osw signal simulated by the model for the present day in the North Indian region (Roche and Caley, 2013). Explanations for the observed North Indian Ocean enrichment in δ^{18}Osw at the LGM could be (1) a contraction of the Indian subtropical gyre and reduction of Agulhas leakage salty water (Caley et al., 2011a) and/or (2) an overall reduction of the hydrological cycle over the western and northern Asian region, in agreement with numerous Indo-Asian monsoonal reconstructions (Schulz et al., 1998; Iwamoto and Inouchi, 2007; Cheng et al., 2009; Guo et al., 2009; Caley et al., 2011b, c; Chabangborn et al., 2013).

Also interesting is the low calcite δ^{18}O anomaly observed in the China Sea (Figs. 8 and 10). This signal cannot be explained by a temperature effect as we observe a cooling more important in the China Sea in comparison to the North Indian Ocean (Figs. 5 and 10). Therefore, we hypothesize an important decrease of the $\Delta\delta^{18}$Osw, a pattern exhibited in our model (Fig. 10c). The cause for such important decrease of the $\Delta\delta^{18}$Osw is not completely clear because the monsoon in East Asia is rather reduced during the LGM (Iwamoto and Inouchi, 2007; Cheng et al., 2009; Guo et al., 2009). Nonetheless, some studies argue for substantial precipitation during the LGM in the South China Sea (Sun et al., 2000; Colin et al., 2010; Chabangborn et al., 2013). Indeed, part of the explanation could reside in the negative δ^{18}O anomaly observed in precipitation over the China Sea (Fig. 1).

The use of calcite δ^{18}O anomalies in the tropical regions (30° N–30° S) do not allow the confirmation of the presence of west–east SST gradients within each basin as the amount of data is rather limited.

As discussed previously, the North Atlantic region exhibits steep calcite δ^{18}O gradients that are also reflected in SST conditions (Figs. 8 and 9). However, large discrepancies remain with respect to reconstructed glacial temperatures based on different microfossil proxies (dinocysts and planktic foraminifera transfer function, alkenones and Mg / Ca ratio measurement on planktic foraminifera) in this region and there was no objective way to reconcile the divergent proxy results (MARGO Project Members, 2009). Our data–model comparison study of the calcite δ^{18}O signal can shed light on these discrepancies. We therefore focused on the North Atlantic and realized data–model comparison for

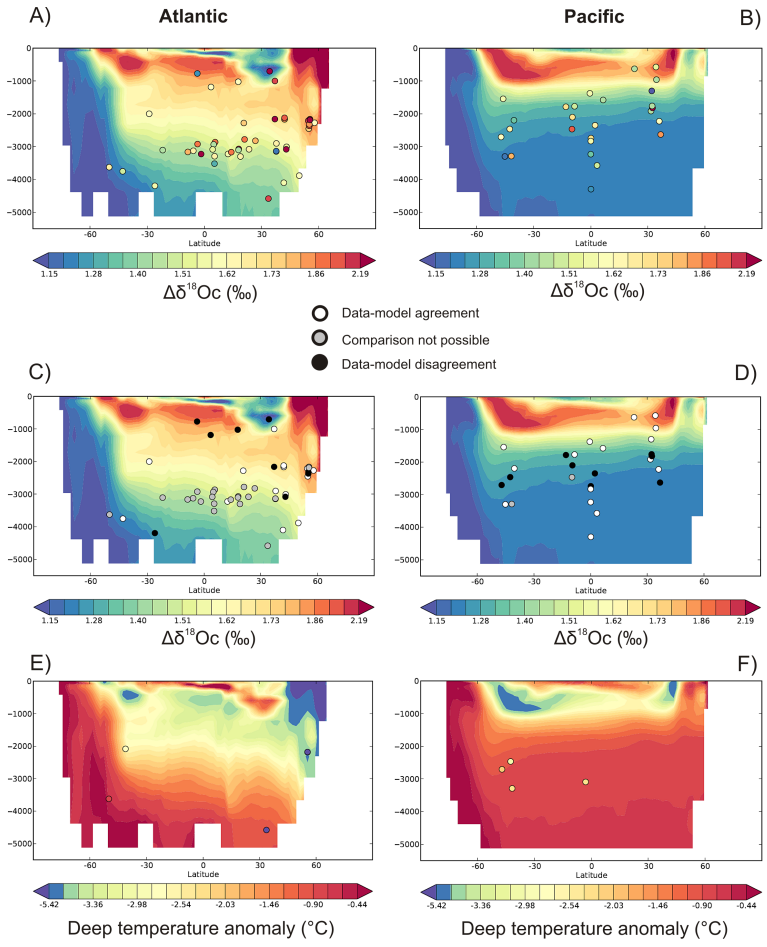

Figure 13. Atlantic and Pacific zonal mean anomaly (LGM-CT) for **(a)** Atlantic and **(b)** Pacific simulated deep ocean calcite δ^{18}O in *i*LOVECLIM and global benthic foraminifera data (Table S2); **(c)** and **(d)** same as **(a)** and **(b)** but taking into account the uncertainties on calcite δ^{18}O data (2σ). Grey points (comparison not possible) denote the absence of error bars on data or denote locations where model results are not comparable to data (coastal sites). **(e)** and **(f)** Simulated deep temperature in *i*LOVECLIM and deep temperature reconstructions for the Atlantic and for the Pacific Oceans respectively (Adkins et al., 2002; Waelbroeck et al., 2002; Malone et al., 2004; Siddall et al., 2010; Elderfield et al., 2012). For colour scale generation explanations see Fig. 1 caption.

calcite δ^{18}O and SST signals (Fig. 11). The main difference between MARGO SST reconstructions and *i*LOVECLIM results corresponds to proxy reconstructions showing a positive SST anomaly in the region located south of the Iceland and Greenland ice sheet. This positive anomaly disagrees with our model results but also with other proxy reconstructions (foraminifera transfer function) indicating an important cooling in the region during the LGM (Fig. 11a).

The calcite δ^{18}O signal is strongly influenced by SST changes in the region and there is very good agreement between model and planktic foraminifera calcite data (Fig. 11). Gradients in calcite δ^{18}O thus mirror SST changes.

In the South Iceland and Greenland region, data and model indicate large positive calcite δ^{18}O anomalies (> 2 ‰) (Fig. 11b). These anomalies can solely be explained by a large negative SST anomaly. Therefore, the data indicating a positive anomaly or a weak cooling in the region are probably biased. After investigation, these data correspond to alkenones and, to a lesser extent, dinocyst reconstructions (Fig. 11a). Positive anomalies derived from dinocyst transfer functions have been interpreted as representing a "no-analogue" situation under partial sea ice coverage and glacial wind fields or a fine stratified layer that becomes warmer in summer (de Vernal et al., 2006). Concerning alkenones, several hypotheses can be proposed to explain the observed discrepancy. First, reconstructions are biased toward a specific season and cannot be directly compared with our mean annual results (Rosell-Melé and Prahl, 2013). Second, culture studies of G. oceanica and E. huxleyi (Conte et al., 1998) together with measurements of sinking particulate matter from Bermuda (Conte et al., 2001) suggest that the real shape of the alkenone–SST is probably sigmoidal, i.e. the calibration of the alkenone index converges asymptotically toward 0 and 1, for low and high temperatures, respectively (Conte et al.,

2006). This could explain a bias with alkenone reconstructions at very low temperature. Finally, several early studies have noticed that alkenone–SST records are affected by laterally advected allochtonous input (Benthien and Müller, 2000; Mollenhauer et al., 2006; Rühlemann and Butzin, 2006). Anomalously warm SST during the last glacial period were observed in a marine sediment core recovered from the South East Indian Ridge (SEIR) at the location of the modern Subantarctic Front and attributed to a strong advection of detrital alkenones produced in warmer surface waters from the Agulhas region to SEIR (Sicre et al., 2005).

These different hypotheses require further investigation in the region. Based on data–model comparison for oxygen stable isotopes, we argue for a strong mean annual temperature anomaly between the LGM and present in the south of the Iceland and Greenland region ($> 6\,^{\circ}C$), supporting the foraminifera transfer function reconstruction.

3.2.2 Oxygen stable isotopes in deep ocean carbonates (benthic foraminifera)

Modelled results for δ^{18}Osw changes in the ocean are presented on Fig. 12 for the deep Atlantic and Pacific Oceans after correction of the LGM ice sheet contribution (1 ‰) (Schrag et al., 1996; Duplessy et al., 2002). Spatial differences in term of δ^{18}Osw anomaly can be observed, suggesting that changes are not homogeneous in the deep ocean. This is in agreement with reconstructions derived from pore fluids in deep-sea sediments (Adkins et al., 2002; Schrag et al., 2002; Malone et al., 2004) (Fig. 12a). Considering the uncertainties on pore fluids reconstructions (0.1 ‰) (Adkins et al., 2002; Schrag et al., 2002), the data point that exhibits a negative δ^{18}Osw anomaly in the deep Atlantic (~ 4500 m) is the only measurement in significant disagreement with the model results (Fig. 12a). The value of this data point is surprising as it would imply a vigorous and/or deeper extension of the North Atlantic deep water at the LGM, in disagreement with reconstructions based on δ^{13}C and Cd / Ca proxies (Lynch-Stieglitz et al., 2007 and references therein) and with our model results. It could also be caused by not depleted enough deep waters at the formation site. However, two data points in the northern North Atlantic are indicating a correct range of values there. Future sensitivity experiments to different glacial circulations are necessary to determine whether the obtained pattern is robust to circulations changes.

Qualitative and quantitative comparison of calcite δ^{18}O anomaly, calculated with the model and benthic foraminifera data with associated error bars (2σ) (Table S2), are visible in Fig. 13a–d for the deep Atlantic and Pacific oceans. Some discrepancies can be observed between data and model and are particularly marked in the equatorial Atlantic at ~ 1000 m, the deep Southern Ocean and central Pacific. The calcite δ^{18}O anomaly is influenced by temperature. The modelled deep-water temperature for the present is around $2\,^{\circ}C$ lower than the data, a pattern particularly marked in the Southern Ocean (Caley and Roche, 2013). This introduces bias into our data–model comparison. The uses of anomalies only slightly limit such bias because deep LGM temperatures are close to the freezing point of seawater at the ocean surface (Adkins et al., 2002).

Reconstructions of past deep temperature are rather rare and localized. The North Atlantic, South Indian and equatorial Pacific are marked by negative temperature anomalies of ~ 4, 3 and $2\,^{\circ}C$ respectively between the LGM and the present (Adkins et al., 2002; Waelbroeck et al., 2002; Siddall et al., 2010) (Fig. 13e and f). Similarly, reconstruction of deep temperature anomaly in the South Pacific yields $\sim 2\,^{\circ}C$ (Malone et al., 2004; Elderfield et al., 2012) (Fig. 13f). The modelled deep temperature anomalies are in good agreement for the North Atlantic at 2000 but not at 4500 m as for the δ^{18}Osw anomaly. For the Southern Ocean and deep equatorial Pacific, the negative anomalies between the LGM and present are about $1\,^{\circ}C$ too weak in the model (Fig. 13f).

Although there are some discrepancies between modelled and measured deep-water temperature, our data–model comparison supports a heterogeneous cooling of a few degrees ($2–4\,^{\circ}C$) in the LGM Ocean.

4 Conclusions

We used the fully coupled atmosphere–ocean three-dimensional model of intermediate complexity *i*LOVECLIM to simulate the climate and oxygen stable isotopes (δ^{18}O) in the atmospheric and oceanic component during the LGM. We also realized a careful compilation of global oxygen isotopic data sets to assess the model performance and constrain the LGM climate. Model results for the annual mean precipitation δ^{18}O show more depleted values in the northern and southern high latitudes during the LGM than at present. The simulated spatial gradient in precipitation δ^{18}O over Greenland is in very good agreement with ice core records. We observe a general pattern toward more enriched calcite δ^{18}O in the model over the continents at the LGM, in agreement with speleothem data. This can be explained by both a general atmospheric cooling in the tropical and subtropical regions and a reduction in precipitation, as confirmed by reconstructions derived from pollens and plant macrofossils (Bartlein et al., 2011). The good agreement between data and model results in terms of annual mean calcite δ^{18}O anomaly offers new perspectives for the understanding of speleothems records covering glacial–interglacial timescales. Long-term transient simulations of water isotopes with *i*LOVECLIM are planned in the near future and the relationship between precipitation δ^{18}O and climate variables such as temperature and precipitation will be investigated.

Data–model comparison for SST indicates that *i*LOVECLIM is capable to satisfyingly simulate oceanic surface conditions at the LGM, whereas the majority of AOGCM simulations experience some difficulties (Braconnot et

al., 2007a). Large discrepancies with respect to glacial temperatures recorded by different microfossil proxies remain in the North Atlantic region and there was no objective way to reconcile the divergent proxy results (MARGO Project Members, 2009). Our data–model comparison for planktic foraminiferal calcite δ^{18}O indicates that a strong mean annual cooling in the area south of Iceland and Greenland characterized the LGM with respect to the present (> 6 °C), supporting the foraminifera transfer function reconstruction but in disagreement with alkenones and dinocyst reconstructions. The data–model comparison also reveals large positive calcite δ^{18}O anomalies in the Southern Ocean linked to an important cooling that could be linked to a reorganization of frontal systems during the LGM. Nonetheless, the exact driver of this pattern remains unclear. From our data–model comparison of planktic foraminifer oxygen stable isotopes and SST we deduced a large positive/negative δ^{18}Osw anomaly for the North Indian Ocean/China Sea between the LGM and the present which may be explained by changes in the hydrological cycle over the region.

Our simulation of the deep ocean suggests that changes in δ^{18}Osw between the LGM and the present are not spatially homogeneous. This is supported by reconstructions derived from pore fluids in deep-sea sediments. The model underestimates the deep ocean cooling thus biasing the comparison with benthic calcite δ^{18}O data. Some experiments are planned in the near future to try modifying this aspect in the model. Nonetheless, our data–model comparison supports a heterogeneous cooling of a few degrees (2–4 °C) in the LGM Ocean.

*i*LOVECLIM reproduces well the δ^{18}O signals between the LGM and present and therefore illustrates how data–model comparison for oxygen isotopes can serve to evaluate a model's capability to simulate a climate that is drastically different from that of the present day.

The Supplement related to this article is available online at doi:10.5194/cp-10-1939-2014-supplement.

Acknowledgements. T. Caley is supported by NWO through the VIDI/AC2ME project no. 864.09.013. D. M. Roche is supported by NWO through the VIDI/AC2ME project no. 864.09.013 and by CNRS-INSU. Two anonymous reviewers and the editor André Paul are acknowledged for useful comments that helped improve the paper. Institut Pierre Simon Laplace is gratefully acknowledged for hosting the *i*LOVECLIM model code under the LUDUS framework project (https://forge.ipsl.jussieu.fr/ludus). This is NWO/AC2ME contribution number 04.

Edited by: A. Paul

References

Adkins, J. F., Mclntyre, K., and Schrag, D.: The salinity, temperature and δ^{18}O of the glacial deep ocean, Science 298, 1769–1773, 2002.

Baertschi, P.: Absolute ^{18}O content of Standard Mean Ocean Water, Earth Planet. Sci. Lett. 31, 341–44, 1976.

Bard, E. and Rickaby, E. M.: Migration of the subtropical front as a modulator of glacial climate, Nature, 460, 380–383, 2009.

Bartlein, P. J., Harrison, S. P., Brewer, S., Connor, S., Davis, B. A. S., Gajewski, K., Guiot, J., Harrison-Prentice, T. I., Henderson, A., Peyron, O., Prentice, I. C., Scholze, M., Seppa, H., Shuman, B., Sugita, S., Thompson, R. S., Viau, A. E., Williams, J., and Wu., H.: Pollen-based continental climate reconstructions at 6 and 21 ka: a global synthesis, Clim. Dynam., 37, 1–28, doi:10.1007/s00382-010-0904-1, 2011.

Benthien, A. and Müller, P. J.: Anomalously low alkenone temperatures caused by lateral particle and sediment transport in the Malvinas Current region, western Argentine Basin, Deep-Sea Res. Pt. I, 47, 2369–2393, 2000.

Berger, A. and Loutre, M.: Astronomical solutions for palaeoclimate studies over the last 3 millions years, Earth Planet. Sci. Lett., 111, 369–382, 1992.

Braconnot, P., Otto-Bliesner, B., Harrison, S., Joussaume, S., Peterchmitt, J.-Y., Abe-Ouchi, A., Crucifix, M., Driesschaert, E., Fichefet, Th., Hewitt, C. D., Kageyama, M., Kitoh, A., Laîné, A., Loutre, M.-F., Marti, O., Merkel, U., Ramstein, G., Valdes, P., Weber, S. L., Yu, Y., and Zhao, Y.: Results of PMIP2 coupled simulations of the Mid-Holocene and Last Glacial Maximum – Part 1: experiments and large-scale features, Clim. Past, 3, 261–277, doi:10.5194/cp-3-261-2007, 2007a.

Braconnot, P., Otto-Bliesner, B., Harrison, S., Joussaume, S., Peterchmitt, J.-Y., Abe-Ouchi, A., Crucifix, M., Driesschaert, E., Fichefet, Th., Hewitt, C. D., Kageyama, M., Kitoh, A., Loutre, M.-F., Marti, O., Merkel, U., Ramstein, G., Valdes, P., Weber, L., Yu, Y., and Zhao, Y.: Results of PMIP2 coupled simulations of the Mid-Holocene and Last Glacial Maximum – Part 2: feedbacks with emphasis on the location of the ITCZ and mid- and high latitudes heat budget, Clim. Past, 3, 279–296, doi:10.5194/cp-3-279-2007, 2007b.

Braconnot, P., Harrison, S. P., Kageyama, M., Bartlein, P. J., Masson-Delmotte, V., Abe-Ouchi, A., Otto-Bliesner, B., and Zhao, Y.: Evaluation of climate models using palaeoclimatic data, Nature Climate Change, 2, 417–424, doi:10.1038/nclimate1456, 2012.

Caley, T. and Roche, D. M.: δ^{18}O water isotope in the *i*LOVECLIM model (version 1.0) – Part 3: A palaeo-perspective based on present-day data-model comparison for oxygen stable isotopes in carbonates, Geosci. Model Dev., 6, 1505–1516, doi:10.5194/gmd-6-1505-2013, 2013.

Caley, T., Kim, J.-H., Malaizé, B., Giraudeau, J., Laepple, T., Caillon, N., Charlier, K., Rebaubier, H., Rossignol, L., Castañeda, I. S., Schouten, S., and Sinninghe Damsté, J. S.: High-latitude obliquity as a dominant forcing in the Agulhas current system, Clim. Past, 7, 1285–1296, doi:10.5194/cp-7-1285-2011, 2011a.

Caley, T., Malaize, B., Zaragosi, S., Rossignol, L., Bourget, J., Eynaud, F., Martinez, P., Giraudeau, J., Charlier, K., and Ellouz-Zimmermann, N.: New Arabian Sea records help decipher orbital timing of Indo-Asian monsoon, Earth Planet. Sc. Lett., 433–444, doi:10.1016/j.epsl.2011.06.019, 2011b.

Caley, T., Malaizé, B., Revel, M., Ducassou, E., Wainer, K., Ibrahim, M., Shoeaib, D., Migeaon, S., and Marieu, V.: Orbital timing of the Indian, East Asian and African boreal monsoons and the concept of a "global monsoon", Quaternary Sci. Rev., 30, 3705–3715, 2011c.

Caley, T., Giraudeau, J., Malaizé, B., Rossignol, L., and Pierre, C.: Agulhas leakage as a key process in the modes of Quaternary climate changes, P. Ntl. Acad. Sci. USA, 109, 6835–6839, 2012.

Chabangborn, A., Brandefelt, J., and Wohlfarth, B.: Asian monsoon climate during the Last Glacial Maximum: palaeo-data–model comparisons, Boreas, 43, 220–242, doi:10.1111/bor.12032, 2013.

Cheng, H., Edwards, R. L., Broecker, W. S., Denton, G. H., Kong, X., Wang, Y., Zhang, R., and Wang, X.: Ice age terminations, Science, 326, 248–252, 2009.

CLIMAP: Seasonal reconstructions of the Earth's surface at the last glacial maximum, Map and Chart Ser., 36, Geological Society of America, 1981.

Colin, C., Siani, G., Sicre, M. A., and Liu, Z.: Impact of the East Asian monsoon rainfall changes on the erosion of the Mekong River basin over the past 25000 yr, Mar. Geol., 271, 84–92, 2010.

Conte, M. H., Thompson, A., Lesley, D., and Harris, R. P.: Genetic and physiological influences on the alkenone/alkenoate versus growth temperature relationship in Emiliania huxleyi and Gephyrocapsa oceanica, Geochim. Cosmochim. Acta, 62, 51–68, 1998.

Conte, M. H., Weber, J.C., King, L. L., and Wakeham, S. G.: The alkenone temperature signal in western North Atlantic surface waters, Geochim. Cosmochim. Acta, 65, 4275–4287, 2001.

Conte, M. H., Sicre, M. A., Rühlemann, C., Weber, J. C., Schulte, S., Schulz-Bull, D., and Blanz, T.: Global temperature calibration of the alkenone unsaturation index (UK'37) in surface waters and comparison with surface sediments, Geochem. Geophy. Geosy., 7, Q02005. doi:10.1029/2005GC001054, 2006.

Craig, H.: Isotopic standards for carbon and oxygen and correction factors for mass-spectrometric analysis of carbon dioxide, Geochim. Cosmochim. Ac., 12, 133–149, 1957.

Craig, H. and Gordon, L. I.: Deuterium and oxygen 18 variations in the ocean and the marine atmosphere, in: Stable Isotopes in Oceanographic Studies and Paleotemperatures, edited by: Tongiorgi, E., Consiglio nazionale delle ricerche, Spoleto, 9–122, 1965.

Crucifix, M., Braconnot, P., Harrison, S., and Otto-Bliesner, B.: Second phase of Palaeoclimate Modelling Intercomparison Project, EOS Trans AGU, 86, 264–265, 2005.

Daeron, M., Guo, W., Eiler, J., Genty, D., Blamart, D., Boch, R., Drysdale, R., Maire, K., Wainer, G., and Zanchetta, G.: $^{13}C^{18}O$ clumping in speleothems: observations from natural caves and precipitation experiments, Geochim. Cosmochim. Acta, 75, 3303–3317, 2011.

Dällenbach, A., Blunier, T., Fluckiger, J., Stauffer, B., Chappellaz, J., and Raynaud, D.: Changes in the atmospheric CH4 gradient between Greenland and Antarctica during the Last Glacial and the transition to the Holocene, Geophys. Res. Lett., 27, 1005–1008, doi:10.1029/1999GL010873, 2000.

Delaygue, G., Jouzel, J., and Dutay, J. C.: Oxygen 18-salinity relationship simulated by an oceanic general circulation model, Earth Planet. Sci. Lett., 178, 113–123, doi:10.1016/S0012-821X(00)00073-X, 2000.

De Vernal, A., Rosell-Melé, A., Kucera, M., Hillaire-Marcel, C., Eynaud, F., Weinelt, M., Dokken, T., and Kageyama, M.: Comparing proxies for the reconstruction of LGM sea-surface conditions in the northern North Atlantic, Quaternary Sci. Rev. 25, 2820–2834, 2006.

Duplessy, J. C., Labeyrie, L., and Waelbroeck, C.: Constraints on the ocean oxygen isotopic enrichment between the Last Glacial Maximum and the Holocene: Paleoceanographic implications, Quaternary Sci. Rev., 21, 315–330, 2002.

Elderfield, H., Ferretti, P., Greaves, M., Crowhurst, S., McCave, I. N., Hodell, D., and Piotrowski, A. M.: Evolution of ocean temperature and ice volume through the Mid-Pleistocene climate transition, Science, 337, 704–709, 2012.

Fluckiger, J., Dällenbach, A., Blunier, T., Stauffer, B., Stocker, T., Raynaud, D., and Barnola, J.-M.: Variations in Atmospheric N_2O Concentration During Abrupt Climatic Changes, Science, 285, 227–230, doi:10.1126/science.285.5425.227, 1999.

Goosse, H., Brovkin, V., Fichefet, T., Haarsma, R., Huybrechts, P., Jongma, J., Mouchet, A., Selten, F., Barriat, P.-Y., Campin, J.-M., Deleersnijder, E., Driesschaert, E., Goelzer, H., Janssens, I., Loutre, M.-F., Morales Maqueda, M. A., Opsteegh, T., Mathieu, P.-P., Munhoven, G., Pettersson, E. J., Renssen, H., Roche, D. M., Schaeffer, M., Tartinville, B., Timmermann, A., and Weber, S. L.: Description of the Earth system model of intermediate complexity LOVECLIM version 1.2, Geosci. Model Dev., 3, 603–633, doi:10.5194/gmd-3-603-2010, 2010.

Guo, Z. T., Berger, A., Yin, Q. Z., and Qin, L.: Strong asymmetry of hemispheric climates during MIS-13 inferred from correlating China loess and Antarctica ice records, Clim. Past, 5, 21–31, doi:10.5194/cp-5-21-2009, 2009.

Hendy, C. H.: The isotopic geochemistry of speleothems, 1. The calculation of the effects of different modes of formation on the isotopic composition of speleothems and their applicability as palaeoclimatic indicators, Geochim. Cosmochim. Ac. 35, 801–824, 1971.

Hoffmann, G., Werner, M., and Heimann, M.: Water isotope module of the ECHAM atmospheric general circulation model: A study on timescales from days to several years, J. Geophys. Res. 103, 16871–16896, 1998.

Iwamoto, N. and Inouchi, Y.: Reconstruction of millennial-scale variations in the East Asian summer monsoon over the past 300 ka based on the total carbon content of sediment from Lake Biwa, Japan, Environ. Geol., 52, 1607–1616, 2007.

Joussaume, S. and Jouzel, J.: Palaeoclimatic tracers: An investigation using an atmospheric general circulation model under ice age conditions: 2. Water isotopes, J. Geophys. Res., 98, 2807–2830, 1993.

Joussaume, S. and Taylor, K.: Palaeoclimate Modelling Intercomparison Project (PMIP), WCRP-111, WMO/TD-No. 1007, 9–24, 2000.

Jouzel, J., Koster, R. D., Suozzo, R. J., Russel, G. L., White, J. W. C., and Broecker, W. S.: Simulations of the HDO and H218O atmospheric cycles using the NASA GISS General Circulation Model: The seasonal cycle for present-day conditions, J. Geophys. Res. 92, 14739–14760, 1987.

Jouzel, J., Hoffmann, G., Koster, R. D., and Masson, V.: Water isotopes in precipitation: Data/model comparison for present-day and past climates, Quat. Sci. Rev., 19, 363–379, 2000.

Kim, S.-T. and O'Neil, J. R.: Equilibrium and nonequilibrium oxygen isotope effects in synthetic carbonates, Geochim. Cosmochim. Ac., 61, 3461–3475, 1997.

Kohfeld, K. E., Graham, R. M., de Boer, A. M., Sime, L. C., Wolff, E. W., Le Quéré, C., and Bopp, L.: Southern Hemisphere westerly wind changes during the Last Glacial Maximum: paleo-data synthesis, Quaternary Sci. Rev., 68, 76–95, 2013.

Kucera, M., Rosell-Melé, A., Schneider, R., Waelbroeck, C., and Weinelte, M.: Multiproxy approach for the reconstruction of the glacial ocean surface (MARGO), Quat. Sci. Rev., 24, 813–819, doi:10.1016/j.quascirev.2004.07.017, 2005.

Lambeck, K. and Chappell, J.: Sea Level Change Through the Last Glacial Cycle, Science, 292, 679–686, 2001.

Lee, J.-E., Fung, I., De Paolo, D., and Fennig, C. C.: Analysis of the global distribution of water isotopes using the NCAR atmospheric general circulation model, J. Geophys. Res., 112, D16306, doi:10.1029/2006JD007657, 2007.

LeGrande, A. N. and Schmidt, G. A.: Water isotopologues as a Quantitative Palaeosalinity Proxy, Palaeoceanography, 26, PA3225, doi:10.1029/2010PA002043, 2011.

Lewis, S. C., LeGrande, A. N., Kelley, M., and Schmidt, G. A.: Water vapour source impacts on oxygen isotope variability in tropical precipitation during Heinrich events, Clim. Past, 6, 325–343, doi:10.5194/cp-6-325-2010, 2010.

Lynch-Stieglitz, J., Adkins, J. F., Curry, W. B., Dokken, T., Hall, I. R., Herguera, J. C., Hirschi, J. J. M., Ivanova, E. V., Kissel, C., Marchal, O., Marchitto, T. M., McCave, I. N., McManus, J. F., Mulitza, S., Ninnemann, U., Peeters, F., Yu, E-F., and Zahn, R.: Atlantic meridional overturning circulation during the Last Glacial Maximum, Science 316, 66–69, 2007.

Malone, M. J., Martin, J. B., Schönfeld, J., Ninnemann, U. S., Nürnburg, D., and White, T. S.: The oxygen isotopic composition and temperature of Southern Ocean bottom waters during the last glacial maximum, Earth Planet. Sc. Lett., 222, 275–283, 2004.

MARGO Project Members, Waelbroeck, C., Paul, A., Kucera, M., Rosell-Melee, A., Weinelt, M., Schneider, R., Mix, A.C., Abelmann, A., Armand, L., Bard, E., Barker, S., Barrows, T. T., Benway, H., Cacho, I., Chen, M. T., Cortijo, E., Crosta, X., de Vernal, A., Dokken, T., Duprat, J., Elderfield, H., Eynaud, F., Gersonde, R., Hayes, A., Henry, M., Hillaire-Marcel, C., Huang, C.C., Jansen, E., Juggins, S., Kallel, N., Kiefer, T., Kienast, M., Labeyrie, L., Leclaire, H., Londeix, L., Mangin, S., Matthiessen, J., Marret, F., Meland, M., Morey, A. E., Mulitza, S., P?aumann, U., Pisias, N. G., Radi, T., Rochon, A., Rohling, E. J., Sbaf?, L., Schafer-Neth, C., Solignac, S., Spero, H., Tachikawa, K., Turon, J. L., and Members, M. P.: Constraints on the magnitude and patterns of ocean cooling at the Last Glacial Maximum, Nat. Geosci., 2, 127–132, 2009.

Mathieu, R., Pollard, D., Cole, J., White, J. W. C., Webb, R. S., and Thompson, S. L.: Simulation of stable water isotope variations by the GENESIS GCM for modern conditions, J. Geophys. Res., 107, 4037, doi:10.1029/2001JD900255, 2002.

Meland, M. Y., Jansen, E., and Elderfield, H.: Constraints on SST estimates for the Northern North Atlantic/Nordic Seas during the LGM, Quaternary Sci. Rev., 24, 835–852, 2005.

Mickler, P., Stern, L., and Banner, J.: Large kinetic isotope effects in modern speleothems, Geol. Soc. Am. Bull., 118, 65–81, 2006.

Mix, A. C., Bard, E., and Schneider, R.: Environmental processes of the ice age: land, oceans, glaciers (EPILOG), Quaternary Sci. Rev., 20, 627–657, 2001.

Mollenhauer, G., McManus, J. F., Benthien, A., Müller, P. J., and Eglinton, T. I.: Rapid lateral particle transport in the Argentine Basin: molecular ^{14}C and $^{230}Th_{xs}$ evidence, Deep-Sea Res. Pt. I, 53, 1224–1243, 2006.

Monnin, E., Indermuele, A., Daellenbach, A., Flueckiger, J., Stauffer, B., Stocker, T., Raynaud, D., and Barnola, J.-M.: Atmospheric CO_2 Concentrations over the Last Glacial Termination, Science, 291, 112–114, 2001.

Noone, D. and Simmonds, I.: Associations between $\delta^{18}O$ of water and climate parameters in a simulation of atmospheric circulation for 1979–95, J. Clim., 15, 3150–3169, 2002.

Paul, A., Mulitza, S., Patzold, J., and Wolff, T.: Simulation of oxygen isotopes in a global ocean model, in: Use of Proxies in Palaeoceanography: Examples From the South Atlantic, edited by: Fischer, G. and Wefer, G., Springer, New York, 655–686, 1999.

Peltier, W.: Global Glacial Isostasy and the Surface of the Ice-Age Earth: The ICE-5G (VM2) Model and GRACE, Ann. Rev. Earth Planet. Sci., 32, 111–149, doi:10.1146/annurev.earth.32.082503.144359, 2004.

Peeters, F., Acheson, R., Brummer, G. J. A., de Ruijter, W. P. M., Schneider, R. R., Ganssen, G. M., Ufkes, E., and Kroon, D.: Vigorous exchange between the Indian and Atlantic oceans at the end of the past five glacial periods, Nature, 430, 661–665, 2004.

Ramirez, E., Hoffmann, S., Taupin, J. D., Francou, B., Ribstein, P., Caillon, N., Ferron, F. A., Landais, A., Petit, J. R., Pouyaud, B., Schotterer, U., Simoes, J. C., and Stievenard, M.: A new deep ice core from Nevado Illimani (6350 m), Bolivia, Earth Planet. Sc. Lett., 212, 337–350, 2003.

Risi, C., Bony, S., Vimeux, F., and Jouzel, J.: Water stable isotopes in the LMDZ4 general circulation model: Model evaluation for present day and past climates and applications to climatic interpretation of tropical isotopic records, J. Geophys. Res., 115, D12118, doi:10.1029/2009JD013255, 2010.

Roche, D. M.: $\delta^{18}O$ water isotope in the *i*LOVECLIM model (version 1.0) – Part 1: Implementation and verification, Geosci. Model Dev., 6, 1481–1491, doi:10.5194/gmd-6-1481-2013, 2013.

Roche, D. M. and Caley, T.: $\delta^{18}O$ water isotope in the iLOVECLIM model (version 1.0) – Part 2: Evaluation of model results against observed $\delta^{18}O$ in water samples, Geosci. Model Dev., 6, 1493–1504, doi:10.5194/gmd-6-1493-2013, 2013.

Roche, D., Paillard, D., and Cortijo, E.: Constraints on the duration and freshwater release of Heinrich event 4 through isotope modelling, Nature, 432, 379–382, 2004a.

Roche, D., Paillard, D., Ganopolski, A., and Hoffmann, G.: Oceanic oxygen-18 at the present day and LGM: Equilibrium simulations with a coupled climate model of intermediate complexity, Earth Planet. Sci. Lett., 218, 317–330, 2004b.

Roche, D. M., Dokken, T. M., Goosse, H., Renssen, H., and Weber, S. L.: Climate of the Last Glacial Maximum: sensitivity studies and model-data comparison with the LOVECLIM coupled model, Clim. Past, 3, 205–224, doi:10.5194/cp-3-205-2007, 2007.

Rohling, E. J. and Cooke, S.: Stable oxygen and carbon isotope ratios in foraminiferal carbonate, in: Modern Foraminifera, edited

by: Sen Gupta, B. K., 39–258, Kluwer Acad., Dordrecht, Netherlands, 1999.

Rosell-Melé, A. and Prahl, F. G.: Seasonality of UK′37 temperature estimates as inferred from sediment trap data, Quaternary Sci. Rev., 72, 128–136, 2013.

Rühlemann, C. and Butzin, M.: Alkenone temperature anomalies in the Brazil-Malvinas Confluence area caused by lateral advection of suspented particulate material, Geochem. Geophys. Geosyst., 7, Q10015, doi:10.1029/2006GC001251, 2006.

Sarnthein, M., Gersonde, R., Niebler, S., Pflaumann, U., Spielhagen, R., Thiede, J., Wefer, G., and Weinelt, M.: Overview of Glacial Atlantic Ocean Mapping (GLAMAP 2000), Palaeoceanograhy, 18, 1030, doi:10.1029/2002PA000769, 2003.

Schmidt, G. A.: Oxygen-18 variations in a global ocean model, Geophys. Res. Lett., 25, 1201–1204, 1998.

Schmidt, G. A., Le Grande, A. N., and Hoffmann, G.: Water isotope expressions of intrinsic and forced variability in a coupled ocean-atmosphere model, J. Geophys. Res., 112, D10103, doi:10.1029/2006JD007781, 2007.

Schmidt, G. A., Annan, J. D., Bartlein, P. J., Cook, B. I., Guilyardi, E., Hargreaves, J. C., Harrison, S. P., Kageyama, M., LeGrande, A. N., Konecky, B., Lovejoy, S., Mann, M. E., Masson-Delmotte, V., Risi, C., Thompson, D., Timmermann, A., Tremblay, L.-B., and Yiou, P.: Using palaeo-climate comparisons to constrain future projections in CMIP5, Clim. Past, 10, 221–250, doi:10.5194/cp-10-221-2014, 2014.

Schrag, D. P., Hampt, G., and Murray, D. W.: Pore fluid constraints on the temperature and oxygen isotopic composition of the glacial ocean, Science, 272, 1930–1932, 1996.

Schrag, D. P., Adkins, J. F., McIntyre, K., Alexander, J. L., Hodell, D. A., Charles, C. D., and McManus, J. F.: The oxygen isotopic composition of seawater during the Last Glacial Maximum, Quaternary Sci. Rev. 21, 331–342, 2002.

Schulz, H., von Rad, U., and Erlenkeuser, H.: Correlation between Arabian Sea and Greenland climate oscillations of the past 110000 years, Nature, 393, 54–57, 1998.

Sicre, M. A., Labeyrie, L., Ezat, U., Duprat, J., Turon, J. L., Schmidt, S., Michel, E., and Mazaud, A.: Mid-latitude Southern Indian Ocean response to Northern Hemisphere Heinrich events, Earth Planet. Sc. Lett., 240, 724–731, 2005.

Siddall, M., Hönisch, B., Waelbroeck, C., and Huybers, P.: Changes in deep Pacific temperature during the mid-Pleistocene transition and Quaternary, Quaternary Sci. Rev., 29, 170–181, 2010.

Sime, L. C., Kohfeld, K. E., Le Quéré, C., Wolff, E. W., de Boer, A. M., Graham, R. M., and Bopp, L.: Southern Hemisphere westerly wind changes during the Last Glacial Maximum: model-data comparison, Quaternary Sci. Rev., 64, 104–120, 2013.

Shackleton, N. J.: Attainment of isotopic equilibrium between ocean water and benthonic foraminifera genus Uvigerina: isotopic changes in the ocean during the last glacial, Les méthodes quantitatives d'étude des variations du climat au cours du Pleistocène, Gif-sur-Yvette, Colloque international du CNRS, 219, 203–210, 1974.

Sharp, Z.: Principles of Stable Isotope Geochemistry, Pearson Prentice Hall, Upper Saddle River, NJ, 2007.

Sun, X., Li, X., Luo, Y., and Chen, X.: The vegetation and climate at the last glaciation on the emerged continental shelf of the South China Sea, Palaeogeography, Palaeoclimatology, Palaeoecology, 160, 301–316, 2000.

Thompson, L., Mosley-Thompson, L., Davis, M., Bolzan, J., Yao, T., Gundestrup, N., Wu, X., Klein, L., and Xie, Z.: Holocene-late Pleistocene climatic ice core records from Quinghai-Tibetan Plateau, Science, 246, 474–477, 1989.

Thompson, L. G., Mosley-Thompson, E., Davis, M. E., Lin, P. N., Henderson, K. A., Cole-Dai, J., Bolzan, J. F., and Liu, K. B.: Late glacial stage and Holocene tropical ice core records from Huascaràn, Peru, Science, 269, 46–50, doi:10.1126/science.269.5220.46, 1995.

Thompson, L. G., Davis, M. E., Mosley-Thompson, E., Sowers, T. A., Henderson, K. A., Zagorodnov, V. S., Lin, P.-N., Mikhalenko, V. N., Campen, R. K., Bolzan, J. F., Cole-Dai, J., and Francou, B.: A 25000 year tropical climate history from Bolivian ice cores, Science 282, 1858–1864, 1998.

Thompson, L. G., Mosley-Thompson, E., and Henderson, K. A.: Ice-core palaeoclimate records in tropical South America since the Last Glacial Maximum, J. Quat. Sci., 15, 1579–1600, 2000.

Tindall, J. C., Valdes, P., and Sime, L. C.: Stable water isotopes in HadCM3: Isotopic signature of El Niño-Southern Oscillation and the tropical amount effect, J. Geophys. Res., 114, D04111, doi:10.1029/2008JD010825, 2009.

Urey, H. C.: Thermodynamic properties of isotopic substances, Journal of Chemical Society, 562–581, 1947.

Vandenberghe, J., Renssen, H., Roche, D. M., Goosse, H., Velichko, A. A., Gorbunov, A., and Levavasseur, G.: Eurasian permafrost instability constrained by reduced sea-ice cover, Quaternary Sci. Rev., 34, 16–23, 2012.

Waelbroeck, C., Labeyrie, L., Michel, E., Duplessy, J. C., McManus, J. F., Lambeck, K., Balbon, E., and Labracherie, M.: Sea-level and deep water temperature changes derived from benthic foraminifera isotopic records, Quaternary Sci. Rev., 21, 295–305, 2002.

Waelbroeck, C., Mulitza, S., Spero, H., Dokken, T., Kiefer, T., and Cortijo, E.: A global compilation of Late Holocene planktic foraminiferal δ^{18}O: Relationship between surface water temperature and δ^{18}O, Quaternary Sci. Rev. 24, 853–878, 2005.

Weber, S. L., Drijfhout, S. S., Abe-Ouchi, A., Crucifix, M., Eby, M., Ganopolski, A., Murakami, S., Otto-Bliesner, B., and Peltier, W. R.: The modern and glacial overturning circulation in the Atlantic ocean in PMIP coupled model simulations, Clim. Past, 3, 51-64, doi:10.5194/cp-3-51-2007, 2007.

Werner, M., Mikolajewicz, U., Heimann, M., and Hoffmann, G.: Borehole versus isotope temperatures on Greenland: seasonnality does matter, Geophys. Res. Lett., 27, 723–726, 2000.

Werner, M., Heimann, M., and Hoffmann, G.: Isotopic composition and origin of polar precipitation in present and glacial climate simulations, Tellus B, 53, 53–71, 2001.

Werner, M., Langebroek, P. M., Carlsen, T., Herold, M., and Lohmann, G.: Stable water isotopes in the ECHAM5 general circulation model: Toward high-resolution isotope modeling on global scale, J. Geophys. Res., 116, D15109, doi:10.1029/2011JD015681, 2011.

Xu, X., Werner, M., Butzin, M., and Lohmann, G.: Water isotope variations in the global ocean model MPI-OM, Geosci. Model Dev., 5, 809–818, doi:10.5194/gmd-5-809-2012, 2012.

Yoshimura, K., Kanamitsu, M., Noone, D., and Oki, T.: Historical isotope simulation using reanalysis atmospheric data, J. Geophys. Res., 113, D19108, doi:10.1029/2008JD010074, 2008.

Zarriess, M. and Mackensen, A.: Testing the impact of seasonal phytodetritus deposition on δ^{13}C of epibenthic foraminifer Cibicidoides wuellerstorfi: a 31000 year high-resolution record from the northwest African continental slope, Palaeoceanography, 26, PA2202,doi:10.1029/2010PA001944, 2011.

Zhou, J., Poulsen, C. J., Pollard, D., and White, T. S.: Simulation of modern and middle Cretaceous marine δ^{18}O with an ocean-atmosphere general circulation model, Palaeoceanography, 23, PA3223, doi:10.1029/2008PA001596, 2008.